LM-01K066
July 16, 2001

Neutron Capture and Transmission Measurements and Resonance Parameter Analysis of Samarium

G. Leinweber, J.A. Burke, H.D. Knox, N.J. Drindak, D.W. Mesh, W.T. Haines, R.V. Ballad, R.C. Block, R.E. Slovacek, C.J. Werner, M.J. Trbovich, D.P. Barry, T. Sato

NOTICE

6-12-01

Neutron Capture and Transmission Measurements and Resonance Parameter Analysis of Samarium

G Leinweber,* JA Burke, HD Knox, NJ Drindak, DW Mesh, WT Haines, and RV Ballad
Lockheed Martin Corporation, P.O. Box 1072, Schenectady, New York 12301-1072

and

RC Block, RE Slovacek, CJ Werner,† MJ Trbovich, DP Barry, and T Sato‡
Rensselaer Polytechnic Institute, Environmental and Energy Engineering Department
Troy, New York 12180-3590

June 2001

* E-mail: leinwg@rpi.edu

† Current address: Los Alamos National Laboratory, Los Alamos, New Mexico 87545

‡ Current address: Kyoto University, Kyoto, Japan

Abstract-*The purpose of the present work is to accurately measure the neutron cross sections of samarium. The most significant isotope is ^{149}Sm, which has a large neutron absorption cross section at thermal energies and is a ^{235}U fission product with a 1% yield. Its cross sections are thus of concern to reactor neutronics.*

Neutron capture and transmission measurements were performed by the time-of-flight technique at the Rensselaer Polytechnic Institute (RPI) LINAC facility using metallic and liquid Sm samples. The capture measurements were made at the 25 meter flight station with a multiplicity-type capture detector, and the transmission total cross-section measurements were performed at 15- and 25-meter flight stations with ^{6}Li glass scintillation detectors. Resonance parameters were determined by a combined analysis of six experiments (three capture and three transmission) using the multi-level R-matrix Bayesian code SAMMY version M2.

The significant features of this work are as follows. Dilute samples of samarium nitrate in deuterated water (D_2O) were prepared to measure the strong resonances at 0.1 and 8 eV without saturation. Disk-shaped spectroscopic quartz cells were obtained with parallel inner surfaces to provide a uniform thickness of solution. The diluent feature of the SAMMY program was used to analyze these data. The SAMMY program also includes multiple scattering corrections to capture yield data and resolution functions specific to the RPI facility.

Resonance parameters for all stable isotopes of samarium were deduced for all resonances up to 30 eV. Thermal capture cross-section and capture resonance integral calculations were made using the resultant resonance parameters and were compared to results obtained using resonance parameters from ENDF/B-VI updated through release 3. Extending the definition of the capture resonance integral to include the strong 0.1 eV resonance in ^{149}Sm, present measurements agree within estimated uncertainties with ENDF/B-VI release 3. The thermal capture cross-section was calculated from the present measurements of the resonance parameters and also agrees with ENDF within estimated uncertainties. The present measurements reduce the statistical uncertainties in resonance parameters compared to prior measurements.

I. INTRODUCTION

For many years, the accuracy of measured cross-sections exceeded that of the computer codes used for nuclear reactor calculations. With the increased use of Monte Carlo methods utilizing increased computer memory for more detailed models and greater speed to permit more histories, this situation changed. The accuracy of the cross-section data is now the limiting factor in many of these calculations.

To improve the accuracy of the measured data, the Rensselaer Polytechnic Institute (RPI) Cross-Section Group has been actively involved in upgrading the experimental equipment used in the measurement program at the RPI linear accelerator (LINAC) facility. A high-efficiency, 16-segment, multiplicity-type gamma detector has been developed for use in neutron capture measurements.[1,2] An improved Time-of-Flight (TOF) Analyzer, that is interfaced directly to a data-acquisition computer, has been designed and constructed to achieve high accuracy and handle high count rate measurements.[1] Improved LINAC targets have been developed to provide enhanced neutron production at energies of interest.[3,4,5] Special-purpose data reduction software has been written to manipulate the data arrays, and the state-of-the-art analysis program SAMMY version M2[6] has been obtained from Oak Ridge National Laboratory (ORNL) for neutron resonance parameter determination. The neutron resonance parameters of interest are radiation width, Γ_γ, and neutron width, Γ_n.

Samarium is one in a series of materials that have been measured at the RPI LINAC facility.[7,8,9] One of the highlights of the present experimental program is the use of dilute samarium in solution with heavy water. These liquid samples maintain a uniform atom density of samarium which cannot be manufactured sufficiently thin and uniform from bulk metal or powder. The heavy water has a very low absorption cross-section and causes minimal interference with the Sm cross-section measurement. D_2O has a smooth cross-section over the measured energy range and corrections can easily be made for its presence. Two such samples were made, and they were used to determine the resonance parameters in the very strong ^{149}Sm resonance at 8 eV.

II. EXPERIMENTAL CONDITIONS

Neutrons are generated via photoneutron reactions caused by the approximately 60 MeV pulsed electron beam from the RPI LINAC. The pulse of electrons strikes a water-cooled tantalum target, where electron collisions generate bremsstrahlung (gamma radiation), which in turn produces photoneutrons. The neutrons are moderated and then collimated as they drift down a long flight tube to the sample and detector.[1,10]

The Sm data consist of six measurements (three capture, three transmission) performed from 1997-1999 at the RPI LINAC facility. Table I gives some details of these experiments including target (described below), pulse width, channel widths in regions of interest, and LINAC pulse repetition rate. The photoneutron pulse width is the same as the electron pulse

Table I

Samarium Experimental Details

Experiment Title	Neutron-Producing Target	Electron Pulse Width (ns)	Chan. Width (μs)	Chan. Width (μs)	Pulse Rep. Rate (pulses per s)	Flight Station (m)
Epithermal Transmission	BBT[3]	60	0.125 >23eV	0.25 >6eV	250	25
Thermal Transmission	ETT[4,5]	125	0.25 >3eV	0.5 >0.5eV	25	15
Liquid (8eV) Transmission	ETT	250	0.25 @ 8 eV		250	25
Epithermal Capture	BBT	60	0.125 >23 eV	0.25 >6 eV	250	25
Thermal Capture	ETT	1000	0.25 >1.4eV	8.0 <1.4eV	25	15
Liquid (8eV) Capture	BBT	250	0.375 @ 8 eV		250	25

width given in Table I. A channel width entered in Table I as 0.125 >23 eV indicates that at neutron energies above 23 eV the channel width was 0.125 μs. The last line in Table I gives a channel width of 0.375 μs for the liquid capture measurement. These data were taken with high resolution (0.125 μs channels) and poor statistics in each channel. They were subsequently analyzed as groups of three data points, giving an effective channel width of 0.375 μs.

Two different LINAC targets were employed in the present series of experiments. Epithermal transmission and capture data and liquid capture data at 8 eV were measured using the Bare Bounce Target (BBT).[3] Here the tantalum target is mounted off the electron beam axis, and a 2.54 cm-thick polyethylene moderator is mounted adjacent to it on the neutron beam axis. Neutrons slowed in the moderator are allowed to drift down the flight tube to the detector location. Epithermal measurements were made with a 0.8 cm-thick B_4C overlap filter in-beam to remove any low energy neutrons from a previous pulse.

Transmission and capture measurements in the thermal energy range and the liquid transmission measurement at 8 eV utilized the Enhanced Thermal Target (ETT).[4,5] This target

was designed to enhance higher thermal and sub-thermal neutron flux. The ETT, described in more detail in References 4 and 5, consists of water-cooled tantalum plates with an integral water moderator, a polyethylene moderator on the axis of the neutron beam, and a graphite reflector.

The neutron energy for a detected event is determined using the Time-of-Flight (TOF) technique. The time from the LINAC electron burst, which creates the neutrons, to the time of the detected event defines the flight time of the neutron. Combining this with precise knowledge of the flight path length gives the neutron energy. The TOF analyzer[1] used in these experiments was designed and constructed in-house, and incorporates a 32 MHz crystal-controlled oscillator coupled to a high speed scaler with 22-bit resolution. It operates as a single start/multiple stop device, meaning that a single LINAC burst initiates a countdown cycle, during which any number of detected events causes the analyzer to record an event. The TOF analyzer employs a fixed deadtime of 0.250 μs to read each event. The overall deadtime of the signal processing electronics has been set at 1.125 μs for capture measurements and 0.6 μs for transmission measurements.[1]

The entire data-taking process is controlled by a Hewlett-Packard HP-1000 Model A990 computer. During operation of the experiment, data are transferred from the TOF analyzer to the computer memory via Direct Memory Access (DMA). The data-taking software is completely menu driven and controls the sample changer, sorts the data into individual spectra, and provides on-line display of the data being accumulated. Descriptions of the TOF analyzer, data-taking computer system, data file structure, and data reduction process are provided in Reference 1.

Table II lists the samples used in these experiments. The purity of metal samples was 99.9%. The liquid samples were prepared by dissolving 99.999% pure Sm_2O_3 in D_2NO_3, and then diluted in 99.80% pure D_2O. Capture data from thick samples were useful in weakly-scattering resonances where reliance on the multiple-scattering correction in SAMMY was minimized. All metal samples were natural elemental samarium sealed inside aluminum sample cans. The thickness of aluminum on each of the front and rear faces of each sample was 0.51 mm. The influence of these sample cans, as well as all background, was measured by including empty sample cans in the capture measurement. The liquid samples were needed to analyze the strong 8-eV resonance. The thinnest manufacturable metal sample was 0.025 mm thick. At this thickness the 8-eV resonance is saturated. The liquid samples provided a uniform solution of natural Sm in heavy water. The heavy water minimized non-Sm absorptions. In Table II the equivalent metal thickness of the liquid samples is given in the last two columns. The sample container was a spectroscopic quartz cell with precisely parallel inner walls. A D_2O blank in an equivalent quartz container was included in the liquid sample measurements as a background measurement. The liquid samples used in the capture measurement of the 8-eV resonance were effective because 8 eV neutrons undergoing D_2O collisions lose sufficient energy to mask any resonance structure due to multiple scattering. The D_2O blank gave an estimate of the background, but it was subsequently fitted with SAMMY. Sample characteristics are given in Table III.

Table II

Sm Samples Used

Experiment Title	0.025 mm	0.051 mm	0.127 mm	0.254 mm	0.508 mm	0.889 mm	1.27 mm	2.54 mm	5.08 mm	soln#1 equiv 0.013 mm	soln#2 equiv 0.0036 mm
Epithermal Transmission				X	X	X	X	X	X		
Thermal Transmission	X	X	X	X				X	X		
8 eV Transmission										X	X
Epithermal Capture	X	X	X								
Thermal Capture	X	X	X								
8 eV Capture											X

II.A. Capture Detector

The capture detector is a multiplicity-type scintillation gamma detector containing 16 sections of NaI(Tl), formed into a 30.5-cm diameter X 30.5-cm height (12- X 12-in.) right circular cylinder with a 8.9-cm (3.5-in.) through hole along its axis.[1,2,10] The cylinder is split normal to its axis into two rings, and each ring is divided into 8 equal pie-shaped segments. Each segment is optically isolated in a hermetically sealed aluminum can, and is mounted on an RCA 8575 photomultiplier tube. The total volume of NaI(Tl) is 20 liters. The capture detector used for the present measurements was located at the East beam tube at a flight path 25.56 meters from the BBT for epithermal measurements. This flight path length was determined from measurements of precisely-known uranium resonance energies.[11] The capture detector is located 25.41 m from the ETT for thermal measurements. This flight path length was calibrated using samarium transmission data. The efficiency of the capture detector is assumed to be the same for all Sm isotopes.

Metal samples 5.08 cm in diameter were precisely positioned at the center of the detector by a computer-controlled sample changer. The sample changer accommodates up to eight samples, and moves them into the beam one at a time. The liquid sample was positioned manually. Neutrons that scatter from the sample are absorbed by a hollow cylindrical liner fabricated of boron carbide ceramic to reduce the number of scattered neutrons reaching the detector. The liner uses boron enriched to 99.4 wt% ^{10}B for maximum

neutron absorption. A 15-cm (6-in.)-thick, 7260-kg (16,000-lb) lead shield surrounds the detector to reduce the gamma-ray background. Reference 1 contains a description of the detector and its signal processing electronics.

Table III

Sample Characteristics*

Nominal Sm Thickness mm	Sample Type	Number Density atom/barn	Physical Sample Thickness mm
0.025	metal	9.168×10^{-5} (4.685×10^{-8})	0.025
0.051	metal	1.377×10^{-4} (4.055×10^{-8})	0.051
0.127	metal	3.607×10^{-4} (5.241×10^{-8})	0.127
0.254	metal	7.429×10^{-4} (2.119×10^{-7})	0.254
0.508	metal	1.508×10^{-3} (5.370×10^{-7})	0.508
0.889	metal	2.637×10^{-3} (9.391×10^{-7})	0.889
1.27	metal	3.728×10^{-3} (2.656×10^{-6})	1.27
2.54	metal	7.547×10^{-3} (2.681×10^{-6})	2.54
5.08	metal	1.524×10^{-2} (5.420×10^{-6})	5.08
0.0036	liquid	1.266×10^{-5} (5.610×10^{-9})	10.0
0.013	liquid	4.705×10^{-5} (2.084×10^{-8})	10.0

*Uncertainties (1σ) in parentheses

II.B. Transmission Detectors

In order to obtain total cross-sections, neutron transmission measurements were conducted at the 15-meter and 25-meter flight stations. The 15-meter station contains a 7.62-cm (3-in.) diameter, 0.3-cm thick NE 905 ^{6}Li glass scintillation detector (6.6% lithium, enriched to 95% in ^{6}Li) and is usually used for measurements covering the energy range from 0.001 eV to 20 eV. The 25-meter station contains a 12.70-cm (5-in.) diameter, 1.27-cm thick NE 905 ^{6}Li glass detector and covers the range from 1 eV to 500 eV.

Each detector is coupled to a photomultiplier tube, which is in-line with the flight path. The transmission detector used for the epithermal measurements was located at the center beam tube at a flight path of 25.585 meters from the BBT.[12] The flight path for thermal transmission measurements was 14.973 m.[13] The flight path lengths were deduced from measurements of precisely known uranium resonances.[12]

Transmission samples along with empty sample holders, which are used to measure the open-beam count rate, are mounted on an 8-position computer-controlled sample changer. The transmission function, which is the ratio of the count rate with a sample in the beam to the count rate with samples removed, varies with neutron energy. Each run consists of one complete cycle through the samples, with a predetermined number of LINAC bursts for each sample position. The distribution of bursts per sample position is chosen to minimize the counting statistical error in the transmission.

III. DATA REDUCTION

III.A. Capture Data

A capture experiment typically involves taking several kinds of data. Sample data are taken with up to eight samples mounted on the sample changer. These usually include about four samples of different thickness, a sample to be used for flux normalization, and two or three empty sample holders for background evaluation. Usually 32 TOF spectra are measured for each sample, i.e., 16 spectra of capture data, and 16 spectra of scattering data, resulting in a data file size of approximately 8 MB per run. A minimum of 100 keV gamma energy is required in a detector segment for the data to be counted. Data are recorded as capture events if the total energy deposited in all 16-detector segments exceeds 1 MeV for epithermal and liquid measurements or 2 MeV for thermal measurements. These discriminator settings have been found to reduce background from ^{128}I decay. Data are recorded as scattering events if the total gamma energy deposited falls between 360 and 600 keV. In this energy region lies the 478 keV gamma emitted following an (n,α) reaction in the $^{10}B_4C$ annular detector liner.

The LINAC electron burst widths and the channel widths for the Sm experiments are summarized in Table I. The average accelerator current during the epithermal capture experiment was approximately 37 μA. The average accelerator current during the thermal capture experiment was approximately 7 μA. The average accelerator current on target during the capture experiment with liquid Sm samples was approximately 50 μA. Each of these measurements lasted approximately 72 hours. In order to minimize data loss in the event of an equipment malfunction and to average LINAC beam-intensity fluctuations, an individual run duration of about one hour was used, with multiple runs summed off-line to accumulate the necessary statistical accuracy.

Once accumulated, the time-of-flight data were subjected to a "consistency check" in

which data were accepted only when the recorded detector counts and beam monitor counts fell within a range of statistical fluctuations. Any data where malfunctions occurred were eliminated. Next, all data were dead-time corrected, similar data sets were combined into composite data runs, and these were normalized to the neutron beam fluence using fixed monitor detectors on the same or adjacent beam tubes. Background was determined using normalized data measured with an empty sample holder mounted on the sample changer. Background spectra evaluated in this way were subtracted from the normalized, summed spectra. Finally, the 16 individual multiplicity spectra were summed into a single multiplicity-independent total spectrum.

Processed capture data is expressed as yield. Yield is defined as the number of neutron captures per neutron incident on the sample. Therefore, in addition to the sample data, another set of data was needed to determine the energy profile of the neutron flux. This was done by mounting a thick $^{10}B_4C$ sample in the sample changer and adjusting the total energy threshold to record the 478 keV gamma rays from neutron absorption in ^{10}B. Since the sample used is black at all energies of interest, the boron absorption spectrum provides an accurate representation of the energy profile of the LINAC's neutron beam flux. These flux data give the shape of the neutron beam flux, but not its magnitude. The flux profile was normalized to the same neutron fluence as the capture sample data using beam monitor data. The thermal flux was further normalized to the black 0.1-eV predominantly-capture resonance in Sm. A small correction (0.8%) was made for the scattering in the 0.1-eV normalizing resonance. The epithermal data could not be directly normalized to this resonance because the boron overlap filter significantly cuts off flux below a few eV. The epithermal flux was normalized indirectly by scaling it so that the background-subtracted area under the yield curve in the 15-eV resonance in ^{149}Sm for the 0.127 mm (0.005 in.) sample matched the background-subtracted area under the yield curve in the thermal measurement with the same sample in the same resonance. That is, the same sample at the same resonance energy will have the same yield. The epithermal flux normalization determined in this way agreed with SAMMY fits obtained by varying the normalization.

The flux for the liquid samarium sample measurement was normalized indirectly to the 0.1-eV Sm resonance in a different way. A 0.254-mm-thick Tm foil was attached to the front of the liquid Sm sample, and data were measured at both 250 pps (LINAC pulses per second) and 25 pps. The 25 pps data were taken without the boron overlap filter for the purpose of using the 0.1-eV Sm resonance to determine the flux, and then using the flux to determine the yield in the predominantly-capture 4-eV resonance in Tm. The 250 pps experiment included the same Sm/Tm sample. The flux in the latter experiment was normalized to match the yield in the 4-eV Tm resonance from the 25 pps experiment.

The flux at 250 pps was measured for only a short time and the counting statistics were poor with only about 230 counts per channel near 8 eV. Since flux is known to be a smooth function of time-of-flight, the flux for the liquid sample capture measurements was smoothed using a cubic spline interpolation. The following method was employed to treat the statistical uncertainty at each channel, i.e., each point in time in the smoothed flux. The

statistical uncertainties at each point in time in the raw, unfit flux were known from propagated counting statistics. Random sampling from the measured flux spectrum within the known errors was taken and spline fit. This was repeated 30 times to get 30 observations of the random variable spline fit flux. From the 30 observations a standard deviation was calculated and applied to the original spline fit flux. These uncertainties were propagated into the uncertainties on yield used in subsequent SAMMY calculations. The smoothing process reduced the flux uncertainties by a factor of 7 or 8 from the measured individual TOF channel flux spectrum. The zero-time for capture was determined for the capture experiment by measuring an attenuated gamma flash from the target.

Finally, Y_i, the capture yield in time-of-flight channel i, was calculated by:

$$Y_i = \frac{C_i - B_i}{K\phi_i} \qquad (1)$$

where

- C_i is the dead-time corrected and monitor-normalized counting rate of the sample measurement in counts per second (cps)
- B_i is the monitor-normalized background counting rate in cps
- K is the flux normalization factor, and
- ϕ_i is the unnormalized neutron flux in cps.

Separate beam-monitor detectors including a ^{6}Li glass scintillation detector and a ^{235}U fission chamber were used to monitor neutron intensity. The capture yield for each sample was produced by dividing its monitor-normalized and background-corrected capture spectrum by the normalized neutron flux spectrum. It was this capture yield that provided input to the SAMMY data analysis code[6] that extracted the neutron resonance parameters.

III.B. Transmission Data

The LINAC electron pulse width and the channel widths for the Sm experiments are summarized in Table I. The average accelerator current during the epithermal transmission experiment was approximately 39 μA. The average accelerator current during the thermal transmission experiment was approximately 3.4 μA. The average accelerator current on target during the transmission experiment with liquid Sm samples was approximately 48 μA. Each of these production runs lasted approximately 72 hours.

As with the capture measurements, a transmission measurement consists of many individual runs of about one-hour in duration which are summed off-line to provide the necessary statistical accuracy. Normally, two sample positions were used to measure open

beam count rate, and these were placed at the beginning and middle of each sample cycle. The time split between samples and open beam was optimized to reduce the counting statistics error.

The large amount of data collected in each of the experiments was first run through a statistical consistency check, as discussed earlier, to verify the stability of the LINAC, the in-beam detector, and the beam monitors. The data were then corrected for dead-time, and runs were normalized and summed.

The time-dependent background was obtained with the one-notch/two-notch method.[14] This method employs blacked-out notch filters of single and double material thickness, and the resulting background determined from each was extrapolated to a zero effective material thickness. The measured background was then fitted to a smooth analytical function of time-of-flight for each sample, including the open beam measurement. The resulting analytical expression was used for the background correction. Finally, T_i, the transmission in time-of-flight channel i, was calculated by:

$$T_i = \frac{(C_i^s - K_s B_i - B_s)}{(C_i^o - K_o B_i - B_o)} \qquad (2)$$

where

C^s_i, C^o_i are, respectively, the dead-time corrected and normalized counting rates of the sample and open measurements in cps,

B_i is the time-dependent background counting rate in cps,

B_s, B_o are, respectively, the steady state background counting rates for sample and open measurements in cps, and

K_s, K_o are normalization factors for the sample and open beam time dependent backgrounds.

The normalization factor, K_o, was determined by forcing the smooth analytical background function through a particular notch-extrapolated background point. The Sm sample normalization factor, K_s, was determined by forcing the smooth analytical background function through the saturated resonance at 8 eV.

The zero-time for the transmission experiments was determined by performing a 'gamma flash' experiment. The burst of gamma rays accompanying the neutron burst is detected by the ^{6}Li detector. The centroid of the gamma-flash peak, less the travel time for light to travel the length of the flight path, is defined as the zero time of neutron production.

Fourteen transmission data sets were used in the present analysis. Table II lists the experiments and samples used. Table III gives sample thicknesses and their uncertainties. All samples were natural samarium.

IV. RESULTS

Resonance parameters, Γ_γ and Γ_n, were extracted from the capture and transmission data sets using the multi-level R-matrix Bayesian code SAMMY version M2[6]. The alpha width, Γ_α, is small and was neglected in the analysis. This was a combined transmission and capture analysis, which employed the multiple-scattering and diluent features recently added to SAMMY. Resolution broadening, self shielding, and multiple scattering are phenomena modelled by SAMMY using input parameters and are needed to extract resonance parameters from transmission and capture data.

Resolution broadening refers to the combined effects of the LINAC electron burst width, the time delay in the moderator, the TOF channel width, and the effect of the detector system. Burst width and channel width are entered as SAMMY input parameters. All other components of the resolution function are handled collectively as an analytical function of amplitude versus time whose integral over time is unity. The function describing the RPI LINAC experimental configuration is now an explicit option in SAMMY.

Self-shielding correction accounts for the attenuation of the incident beam in the sample. Multiple scattering correction accounts for the increase in observed capture yield due to capture of neutrons scattered from higher energies. Both corrections were applied in SAMMY for all capture analyses. Thick sample data were used only when a resonance had a small scatter-to-capture ratio and has a poor signal-to-background ratio in thinner sample data.

Table IV lists Sm evaluations from ENDF/B-VI[15] updated through release 3. These are the latest Sm evaluations. Whenever the term ENDF is used in this report, refer to Table IV for the specific evaluation used for each isotope. As a starting point SAMMY fits utilized Sm parameters from the evaluations listed in Table IV. In addition, the 24.7 eV and 28 eV resonances, which do not appear in ENDF, were included. The initial parameters for these resonances were taken from Mughabghab.[16] The Mughabghab parameters are as follows, where E is in eV and $2g\Gamma_n$ is in meV.

E= 24.6 ± 0.1	$2g\Gamma_n$= 0.35 ± 0.02	Γ_γ= unspecified	J= 4	^{149}Sm
E= 28.0 ± 0.1	$2g\Gamma_n$= 0.53 ± 0.03	Γ_γ= unspecified	J= 3	^{149}Sm

Initial fits were made to estimate any background that was not removed during the original data reduction. The function *[A + Bt]*, where *A* and *B* are constants and *t* is time-of-flight, was found to fit the background for all data sets rather well. Therefore, each data set was fitted individually to estimate the background shape in that sample. Next, these background functions were fixed while resonance parameters were varied in a covariance-

Table IV

Summary of Samarium Evaluations

Samarium Isotope	Latest ENDF Evaluation
144	ENDF6.3
147	ENDF6.0
148	ENDF6.0
149	ENDF6.0
150	ENDF6.2
151	ENDF6.1
152	ENDF6.2
154	ENDF6.0

matrix-linked serial calculation including all transmission and capture samples for each energy range, thermal and epithermal. Following these calculations, four resonances, 16, 23, 24, and 28 eV, required individual analysis.

The potential scattering length used for samarium was 8.30 fm.[15] The potential scattering lengths used for deuterium and oxygen in the liquid samples were 5.20 fm and 5.46 fm, respectively. These latter two radii were calculated from potential scattering cross-sections, deuterium σ_s = 3.4 barns, oxygen σ_s = 3.75 barns.[17] The effective temperature was 293 K, and no external R-function was employed. Distant resonances were represented by including all of the resonances present in the ENDF file. No p-wave resonances were observed in the energy range currently being reported. The calculations fitted the resonance energy, E, and the resonance widths, Γ_γ and Γ_n.

The final results of resonance parameter fitting for all resonances up to 30 eV are given in Table V. The results of the present measurements are compared to previous measurements. The last column of Table V gives the neutron width as given in the references where g is the statistical weight factor, $g=(2J+1)/[2(2I+1)]$, J is the angular momentum of the resonance, I is the spin of the nucleus, and Γ_n^0 is the reduced neutron width, $\Gamma_n^0 = \Gamma_n/\sqrt{E}$. Uncertainties are quoted whenever they appear in the references. Statistical uncertainties (1σ) propagated by SAMMY are given for the present measurements in brackets in Table V. Estimated uncertainties on the present measurements are given in parentheses in Table V. The uncertainties in resonance energies for the present measurements include uncertainties in

Table V page 1 of 6

Samarium Resonance Parameters*

Reference	Ref No.	Year	Resonance Energy (eV)	Γ_γ (meV)	Γ_n (meV)	Neutron Width as Reported in Reference (meV)
^{149}Sm abun=13.8% s-wave J=4 g=9/16						
Marshak and Sailor	18	1958	0.0976 (5)	63.6 (10)	0.500 (31)	Γ_n^0=1.6 (1)
Pattenden	19	1958	0.0967 (5)		0.498 (28)	$2g\Gamma_n^0$=1.8 (1)
Sokolowski et al.	20	1964	0.097	64		
Akyuez et al.	21	1968	0.0973	63.5 (13)		
Asami et al.	22	1968	0.0988 (8)	59.0 (8)	0.537 (10)	Γ_n^0=1.71 (3)
present		2001	0.096 (1)	61.6 (7) [1]	0.507 (5) [1]	
^{149}Sm abun=13.8% s-wave J=4 g=9/16						
Pattenden	23	1963	0.873 (3)	65 assumed	0.55 (5)	$2g\Gamma_n^0$=0.66 (6)
Akyuez et al.	21	1968	0.872	63.5 (15)		
present		2001	0.87 (1)	61.8 (7) [2]	0.756 (3) [1]	
^{147}Sm abun=15.0% s-wave J=3 g=7/16						
Pattenden	19	1963	3.42 (2)	65 assumed	1.25 (6)	$2g\Gamma_n^0$=0.59 (3)
Codding et al.	24	1971	3.39	69	1.79	$2g\Gamma_n^0$=0.851
Eiland et al.	25	1974	3.417	67 (8)	1.33 (4)	$g\Gamma_n$=0.584 (15)
Mizumoto	26	1981	3.396	67 (3)	1.35 (2)	$2g\Gamma_n$=1.18 (2)
present		2001	3.40 (1)	63.4 (24) [4]	1.27 (2) [1]	

* Uncertainties given in parentheses are in the least significant digits. Estimated uncertainties in parentheses for present measurements represent the variability of the fitted results. They are on the order of 1σ. Purely statistical Bayesian errors for present measurements are given in brackets.

Samarium Resonance Parameters*

Reference	Ref No.	Year	Resonance Energy (eV)	Γ_γ (meV)	Γ_n (meV)	Neutron Width as Reported in Reference (meV)
^{149}Sm abun=13.8% s-wave J=4 g=9/16						
Mizumoto	26	1981	4.94	59 (2)	2.14 (3)	$2g\Gamma_n$=2.41 (3)
present		2001	4.94 (1)	67.5 (17) [5]	1.85 (16) [1]	
^{149}Sm abun=13.8% s-wave J=3 g=7/16						
Mizumoto	26	1981	6.428	68 (5)	1.20 (2)	$2g\Gamma_n$=1.05 (2)
present		2001	6.43 (1)	56 (13) [2]	0.80 (11) [1]	
^{152}Sm abun=26.7% s-wave J=½ g=1						
Pattenden	23	1963	8.09 (4)	65 assumed	145 (6)	Γ_n^0=51 (2)
Rahn et al.	27	1972	8.06 (1)	60 (11)	130 assumed	Γ_n^0=46 (2)
present		2001	8.03 (1)	70.9 (60) [25]	129 (4) [2]	
^{149}Sm abun=13.8% s-wave J=4 g=9/16						
Anufriev et al.	28	1978	8.96 (2)		9.87 (62)	$2g\Gamma_n$=11.1 (7)
Mizumoto	26	1981	8.928	70 (4)	11.84 (13)	$2g\Gamma_n$=13.32 (14)
present		2001	8.93 (1)	59.3 (90) [58]	8.66 (100) [67]	
^{149}Sm abun=13.8% s-wave J=3 g=7/16						
Mizumoto	26	1981	12.0	62 (6)	1.82 (2)	$2g\Gamma_n$=1.59 (2)
present		2001	12.01 (1)	68.6 (47) [24]	1.86 (5) [2]	

* Uncertainties given in parentheses are in the least significant digits. Estimated uncertainties in parentheses for present measurements represent the variability of the fitted results. They are on the order of 1σ. Purely statistical Bayesian errors for present measurements are given in brackets.

Samarium Resonance Parameters*

Reference	Ref No.	Year	Resonance Energy (eV)	Γ_γ (meV)	Γ_n (meV)	Neutron Width as Reported in Reference (meV)
^{149}Sm abun=13.8% s-wave J=4 g=9/16						
Popov et al.	29	1980	14.89	78 (5)	5.44 (9)	$g\Gamma_n$=3.06 (5)
Mizumoto	26	1981	14.89	65 (8)	5.64 (7)	$2g\Gamma_n$=6.34 (8)
present		2001	14.90 (1)	66.2 (21) [13]	5.64 (6) [4]	
^{149}Sm abun=13.8% s-wave J=3 g=7/16						
Mizumoto	26	1981	15.85		0.37 (2)	$2g\Gamma_n$=0.32 (2)
present		2001	15.88 (1)	85 (30) [6]	0.43 (4) [2]	
^{149}Sm abun=13.8% s-wave J=4 g=9/16						
Popov et al.	29	1980	17.16	94 (5)	2.15 (5)	$g\Gamma_n$=1.21 (3)
Mizumoto	26	1981	17.14		1.98 (4)	$2g\Gamma_n$=2.23 (4)
present		2001	17.16 (1)	83 (30) [4]	2.26 (19) [3]	

* Uncertainties given in parentheses are in the least significant digits. Estimated uncertainties in parentheses for present measurements represent the variability of the fitted results. They are on the order of 1σ. Purely statistical Bayesian errors for present measurements are given in brackets.

Table V page 4 of 6

Samarium Resonance Parameters*

Reference	Ref No.	Year	Resonance Energy (eV)	Γ_γ (meV)	Γ_n (meV)	Neutron Width as Reported in Reference (meV)
^{147}Sm abun=15.0% s-wave J=4 g=9/16						
Codding et al.	24	1971	18.30	78 average of area (73) & shape (83)	66.5	area analysis: $2g\Gamma_n^0$=17.1 shape fit: $2g\Gamma_n^0$=17.9
Eiland et al.	25	1974	18.41	145 (16)	70.8 (3)	$g\Gamma_n$=39.8 (15)
Popov et al.	29	1980	18.34	93 (4)	64 (2)	$g\Gamma_n$=36 (1)
Mizumoto	26	1981	18.32	72 (4)	71.9 (4)	$2g\Gamma_n$=80.9 (4)
Georgiev et al.	30	1993	18.36 (2)			
present		2001	18.32 (1)	64.1 (66) [10]	67.8 (59) [5]	
^{150}Sm abun= 7.4% s-wave J=½ g=1						
Eiland et al.	25	1974	20.7	60.2 (55)	47.3 (15)	
Anufriev et al.	31	1977	20.64 (9)	76 (8)	53 (6)	Γ_{tot}=129 (10) Γ_n=53 (6)
Popov et al.	29	1980	20.59	62 (5)	48 (1)	$g\Gamma_n$=48 (1)
present		2001	20.59 (1)	45.1 (41) [8]	48.9 (16) [4]	
^{149}Sm abun=13.8% s-wave J=4 g=9/16						
Popov et al.	29	1980	23.24	72 (9)	0.89 (4)	$g\Gamma_n$=0.5 (2)
Mizumoto	26	1981	23.23		0.88 (3)	$2g\Gamma_n$=0.99 (3)
present		2001	23.25 (1)	40 (20) [4]	0.78 (3) [2]	

* Uncertainties given in parentheses are in the least significant digits. Estimated uncertainties in parentheses for present measurements represent the variability of the fitted results. They are on the order of 1σ. Purely statistical Bayesian errors for present measurements are given in brackets.

Samarium Resonance Parameters*

Reference	Ref No.	Year	Resonance Energy (eV)	Γ_γ (meV)	Γ_n (meV)	Neutron Width as Reported in Reference (meV)
^{149}Sm abun=13.8% s-wave J=4 g=9/16						
Popov et al.	29	1980	24.72		0.55 (18)	$g\Gamma_n$=0.31 (10)
Mizumoto	26	1981	24.72		0.29 (2)	$2g\Gamma_n$=0.33 (2)
present		2001	24.72 (1)	40 (20) [4]	0.36 (4) [2]	
^{149}Sm abun=13.8% s-wave J=3 g=7/16						
Popov et al.	29	1980	25.28	88 (5)	15.5 (2)	$g\Gamma_n$=6.8 (8)
Mizumoto	26	1981	25.26	69 (14)	15.99 (26)	$2g\Gamma_n$=13.99 (23)
Georgiev et al.	32	1992	25.26	63 (9)		
present		2001	25.27 (1)	61.5 (20) [14]	15.9 (3) [2]	
^{149}Sm abun=13.8% s-wave J=4 g=9/16						
Popov et al.	29	1980	26.11	90 (5)	3.48 (4)	$g\Gamma_n$=1.96 (2)
Mizumoto	26	1981	26.08		3.19 (7)	$2g\Gamma_n$=3.59 (8)
present		2001	26.10 (1)	45.0 (32) [25]	3.27 (5) [4]	

* Uncertainties given in parentheses are in the least significant digits. Estimated uncertainties in parentheses for present measurements represent the variability of the fitted results. They are on the order of 1σ. Purely statistical Bayesian errors for present measurements are given in brackets.

Table V page 6 of 6
Samarium Resonance Parameters*

Reference	Ref No.	Year	Resonance Energy (eV)	Γ_γ (meV)	Γ_n (meV)	Neutron Width as Reported in Reference (meV)
^{147}Sm abun=15.0% s-wave J=3 g=7/16						
Codding et al.	24	1971	27.3	65 assumed	7.94	area analysis: $2g\Gamma_n^0$=1.06 shape fit: $2g\Gamma_n^0$=1.60
Eiland et al.	25	1974	27.28	66 assumed	7.15 (28)	$g\Gamma_n$=3.13 (12)
Popov et al.	29	1980	27.19	84 (7)	6.51 (5)	$g\Gamma_n$=2.85 (2)
Mizumoto	26	1981	27.16		6.95 (13)	$2g\Gamma_n$=80.9 (4)
Georgiev et al.	30	1993	27.16 (2)	84 (5)		
present		2001	27.19 (1)	54.7 (33) [21]	6.34 (7) [5]	
^{149}Sm abun=13.8% s-wave J=3 g=7/16						
Popov et al.	29	1980	28.03		0.62 (23)	$g\Gamma_n$=0.27 (10)
Mizumoto	26	1981	27.98		0.61 (4)	$2g\Gamma_n$=0.53 (3)
present		2001	28.01 (1)	40 (20) [4]	0.52 (2) [2]	
^{147}Sm abun=15.0% s-wave J=3 g=7/16						
Codding et al.	24	1971	29.9	65 assumed	13.4	area analysis: $2g\Gamma_n^0$=1.89 shape fit: $2g\Gamma_n^0$=2.39
Eiland et al.	25	1974	29.88	66 assumed	14.3 (6)	$g\Gamma_n$=6.25 (25)
Popov et al.	29	1980	29.75	104 (10)	15.3 (7)	$g\Gamma_n$=6.7 (3)
Mizumoto	26	1981	29.74	71 (6)	14.7 (2)	$2g\Gamma_n$=12.9 (2)
present		2001	29.80 (1)	89.0 (37) [18]	17.1 (3) [2]	

* Uncertainties given in parentheses are in the least significant digits. Estimated uncertainties in parentheses for present measurements represent the variability of the fitted results. They are on the order of 1σ. Purely statistical Bayesian errors for present measurements are given in brackets.

flight path lengths and zero-time measurements.

Examples comparing the results of present measurements, ENDF[15] parameters, and measured spectra are shown in Figures 1-5. The SAMMY curves represent the results combining multiple samples in both transmission and capture. Details of the data sets are given in Tables I through III. The solid line in each figure represents the SAMMY fit, while the dashed line represents ENDF parameters.

Figure 1 shows final fits for the thermal-through-10-eV region. Resonance parameters for the 0.1, 0.9 and 3.4 eV resonances were fitted using all samples in thermal capture and transmission. For clarity only one of every five or ten data points is shown (see caption to Figure 1). The statistical uncertainties quoted for Γ_n for the present measurements for the 0.1 and 0.9 eV resonances are quite small (<0.001 meV). More realistic estimates of the uncertainties on the resonance parameters are given in parentheses for the present measurements in Table V. These uncertainties represent the stability of the resultant parameters to various combinations of data sets. ENDF[15] gives the parameters for these 3 resonances as E= 0.0981 eV, Γ_γ= 61.7 meV, Γ_n=0.529 meV; E= 0.873 eV, Γ_γ= 59.9 meV, Γ_n=0.724 meV; E= 3.397 eV, Γ_γ= 67.0 meV, Γ_n=1.34 meV.

Figure 2 focuses on the 4-13 eV region. This region was fitted in three pieces. Parameters for the resonances at 5 and 6.4 eV were determined from selected thermal and epithermal data. Thin-sample (less than 0.254 mm) transmission data were omitted because the 5 and 6.4 eV resonances were too weak to analyze at those thicknesses. Thick-sample (>1.27 mm) transmission data were omitted due to near saturation of the 5 eV resonance and interference of the strong 8 eV resonance with the 6.4 eV resonance. Six capture data sets, 0.025, 0.051, and 0.127 mm thick samples from both thermal and epithermal, were included in the 5 and 6.4 eV fit. Also, the local capture background was fitted along with the resonance parameters, although it is the global background fit which is shown in Figure 2. ENDF gives the parameters for these resonances as E= 4.98 eV, Γ_γ= 66.5 meV, Γ_n=2.008 meV; E= 6.48 eV, Γ_γ= 62.0 meV, Γ_n=0.636 meV. The present measurement of Γ_n and Γ_γ for the 5 and 6.4 eV resonances differ substantially from previous measurements; however, all data sets are in agreement that the quoted present values of Γ_n and Γ_γ provide significantly better fits.

Resonance parameters for the 8 and 9 eV resonances were fitted using dilute liquid sample data, not with the data shown in Figure 2. The 8 eV resonance is saturated for even the thinnest (0.025 mm) metal sample. The 8 and 9 eV resonances are shown with liquid sample data in Figure 3. The energies of the 8 and 9 eV resonances were determined from 0.025 mm thermal transmission data. The resonance parameters were determined from both liquid transmission samples and the 0.0036 mm equivalent thickness liquid sample in capture. ENDF gives the parameters for these resonances as E= 8.047 eV, Γ_γ= 66.0 meV, Γ_n=135 meV; E= 8.90 eV, Γ_γ= 58.6 meV, Γ_n= 9.23 meV.

The fit to the 12 and 15 eV resonances, shown in Figures 2 and 4, respectively,

utilized epithermal data only. Three capture data sets, 0.025, 0.051, and 0.127 mm thick samples, were used. The three thinnest epithermal transmission samples, 0.254, 0.508, and 0.889 mm thick, were used. Thicker samples were omitted to avoid saturation. ENDF gives the parameters for these resonances as E= 12.20 eV, Γ_γ= 49.0 meV, Γ_n= 1.40 meV; E= 14.90 eV, Γ_γ= 49.0 meV, Γ_n= 5.90 meV. Table V shows that the current fit of the 12 eV resonance energy agrees better with Mizumoto[26] than with ENDF.

Figure 4 shows the 13-22 eV energy region. A fit including all epithermal samples except 0.254 mm capture gave the results for the 18 and 20 eV resonances shown in Figure 4. ENDF gives the parameters for these resonances as E= 18.30 eV, Γ_γ= 76.0 meV, Γ_n= 70.2 meV; E= 20.65 eV, Γ_γ= 61.0 meV, Γ_n= 47.9 meV.

The 16 eV resonance parameters were determined from only the 5.08 mm transmission and 0.127 mm capture data. ENDF gives the parameters for this resonance as E= 16.00 eV, Γ_γ= 49.0 meV, Γ_n= 0.610 meV. The resonance parameter uncertainties for the 16 eV resonance, as well as three other weak, predominantly capture resonances at 23, 24.7, and 28 eV, are based on the sensitivity of goodness of fit to variations in the resonance parameters. Evidence of the insensitivity of fits to Γ_γ in resonances where $\Gamma_\gamma >> \Gamma_n$ can be seen in the 16 eV resonance where $\Gamma_\gamma = 85 \pm 30$ meV. Although the present measurement of Γ_γ for this resonance is very different from ENDF, the large uncertainty indicates that the ENDF value fits the data nearly as well .

The 17 eV resonance was fit with 0.051 and 0.127 mm capture data and 0.508, 0.889, 1.27, and 2.54 mm transmission data. ENDF gives the parameters for this resonance as E= 17.20 eV, Γ_γ= 49.0 meV, Γ_n= 3.00 meV. Table V shows that the present measurement of Γ_n and Γ_γ for the 17 eV resonance agrees better with Popov et al.[29] than with ENDF.

Figure 5 shows the 22.5 - 30.5 eV region. All epithermal transmission and capture data (except 0.254 mm capture) were used to fit the 25.3, 26, 27, and 29.8 eV resonances. Results are shown in Figure 5. ENDF gives the parameters for these resonances as E= 25.30 eV, Γ_γ= 49.0 meV, Γ_n= 13.8 meV; E= 26.10 eV, Γ_γ= 49.0 meV, Γ_n= 3.20 meV; E= 27.10 eV, Γ_γ= 84.0 meV, Γ_n= 6.80 meV; E= 29.74 eV, Γ_γ= 71.0 meV, Γ_n= 14.7 meV.

The 23 eV resonance was fit to 0.051 and 0.127 mm capture and 1.27, 2.54, and 5.08 mm transmission data. A local background for each capture sample was determined and used while fitting resonance parameters. ENDF gives the parameters for this resonance as E= 23.20 eV, Γ_γ= 49.0 meV, Γ_n= 1.20 meV.

The 24.7 eV resonance parameters were determined from only 2.54 and 5.08 mm transmission and 0.127 mm capture data. The local capture background determined in the 23 eV analysis was also used in the 24.7 eV resonance parameter fit. The 28 eV resonance is another weak resonance fitted with only 2.54 and 5.08 mm transmission and 0.127 mm capture data. A local capture background for the 0.127 mm capture sample was determined during the 28 eV resonance parameter fit. However, it is the global background fit which is

shown in Figure 5. Note that the 24.7 and 28 eV resonances are not present in the ENDF library but are reported in References 26 and 29 and are visible in Figure 5. These two resonances are also identified in Reference 32, but no resonance parameters are provided.

Infinitely dilute capture resonance integrals from the present measurements are compared to those of ENDF in Tables VI and VII. The capture resonance integrals (RI) in Tables VI and VII are defined as:

$$RI = \int_{E_{min}}^{20MeV} \sigma_c(E)\frac{dE}{E} \qquad (3)$$

In Equation (3) $\sigma_C(E)$ is the capture cross-section in barns, E is energy in eV. E_{min} for the standard resonance integrals given in Table VI is 0.5 eV. This is the conventional lower energy cutoff for RI based on the cadmium cutoff. Resonance integrals were calculated using NJOY[35] to integrate the ENDF capture cross-section from 0.5 eV to 20 MeV. This is the value presented for total RI in column 3 of Table VI. Secondly, the contributions to the capture resonance integral from the resonances below 30 eV were calculated from both ENDF values and from the currently-fitted values. The net change due to the present measurements was then added to the NJOY/ENDF capture RI to represent the capture resonance integral due to the present measurements. Zeros in the resonance contribution columns in Tables VI, VII, and VIII indicate that no resonances have been observed in these isotopes below 30 eV. Contributions from ^{151}Sm are included in the tables for completeness, but ^{151}Sm was not part of the present measurement.

Samarium has a very large capture resonance at 0.1 eV. In order to quantify the RI including this resonance, a second RI is defined. The extended resonance integral given in Table VII estimates an RI defined by E_{min} = 0.05 eV. In Table VII the capture RI in column 3 is defined as the NJOY capture RI from column 3 of Table VI plus the contribution from the 0.1 eV resonance based on ENDF parameters. Tables VI and VII show that the resonance integrals calculated using ENDF parameters fall within measurement uncertainties of the present elemental Sm resonance integrals.

Thermal capture cross-sections at 2200 m/s are given in Table VIII. They are calculated using the same method as for the standard capture resonance integral in Table VI. Thermal capture cross-sections given in Table VIII are evaluated at 293K and are calculated with NJOY using ENDF parameters. Then the net change due to individual measured resonances is added to represent the thermal capture cross-section due to present measurements. The 0.1 eV resonance is the major contributor of all resonances accounting for 25600 barns of the 25730 barns given for ^{149}Sm according to present measurements. It contributes 25300 barns of 25500 barns using ENDF/B-VI parameters. The uncertainties

Table VI
Standard Capture Resonance Integral (RI) - Infinitely Dilute 0.5 eV - 20 MeV

Sm Isotope	abun-dance, f_i	capture RI from NJOY & ENDF (b)	Contribution from Resonances < 30 eV (b)			capture RI due to the present measurements (b)
			ENDF	present measurements	net change	
144	0.031	2*	0	0	0	2
147	0.150	790	502	469	-33	757
148	0.113	28	0	0	0	28
149	0.138	3264	2790	2893	103	3367
150	0.074	338	261	230	-31	307
151[a]	0.000	3448	0	0	0	3448
152	0.267	2980	2841	2945	104	3084
154	0.227	34	0	0	0	34
RI for element $\Sigma RI_i f_i$		1400	1238	1273	35	1435
estimated uncertainty in sum				77	77	NA
% uncertainty in sum				6.0	220	NA

* This is a consensus value from the Chart of the Nuclides[33] and JENDL[34]. The result of an NJOY calculation using ENDF parameters is 30 barns.
[a] The ^{151}Sm resonance integral is shown for completeness, although it was not measured here.

Table VII
Extended Capture Resonance Integral (RI) - Infinitely Dilute 0.05 eV - 20 MeV

Sm Isotope	abun-dance, f_i	RI from Table VI NJOY plus 0.1 eV resonance (b)	Contribution from Resonances < 30 eV (b)			capture RI due to the present measurements (b)
			ENDF	present measurements	net change	
144	0.031	2*	0	0	0	2
147	0.150	790	502	469	-33	757
148	0.113	28	0	0	0	28
149	0.138	130600	130100	130300	200	130800
150	0.074	338	261	230	-31	307
151[a]	0.000	3448	0	0	0	3448
152	0.267	2980	2841	2945	104	3084
154	0.227	34	0	0	0	34
RI for element $\sum RI_i f_i$		18970	18810	18860	50	19020
estimated uncertainty in sum				339	339	NA
% uncertainty in sum				1.80	678	NA
% increase in measured resonances						0.26 ± 1.80
% increase in extended resonance integral						0.26 ± NA

* This is a consensus value from the Chart of the Nuclides[33] and JENDL[34]. The result of an NJOY calculation using ENDF parameters is 30 barns.
[a] The ^{151}Sm resonance integral is shown for completeness, although it was not measured here.

quoted in Tables VI, VII, and VIII are propagated from the estimated uncertainties in Γ_n and Γ_γ given in parentheses for the present measurements in Table V. The small increase in thermal capture cross section is within measurement uncertainties of the cross section calculated using ENDF parameters.

Table VIII
Thermal (2200 m/s) Capture Cross-Section ($\sigma_{\gamma th}$)

Sm Isotope	abun-dance, f_i	$\sigma_{\gamma th}$ from NJOY & ENDF (b)	Contribution from Resonances < 30 eV (b)			$\sigma_{\gamma th}$ due to present measurements (b)
			ENDF	present measurements	net change	
144	0.031	2	0	0	0	2
147	0.150	57	17	15	-2	55
148	0.113	3	0	0	0	3
149	0.138	39690	25500	25730	230	39920
150	0.074	104	6	5	-1	103
151*	0.000	15210	0	0	0	15210
152	0.267	206	201	208	7	213
154	0.227	6	0	0	0	6
$\sigma_{\gamma th}$ for element $\sum\sigma_i f_i$		5550	3576	3609	33	5583
estimated uncertainty in sum				53	53	NA
% increase in measured resonances						0.92 ± 1.5
% increase in elemental thermal capture cross-section						$0.59 \pm$ NA

* The ^{151}Sm contribution to thermal capture cross section is shown for completeness, although it was not measured here.

V. DISCUSSION

In Table V, estimated uncertainties (on the order of 1σ) are given for the present measurements in parentheses next to the data values. The purely statistical Bayesian uncertainties appear in Table V in brackets for the present measurements. The statistical uncertainties have been propagated from the data by SAMMY for the entire capture/transmission analysis. The estimated uncertainties represent a more realistic estimate of how well we believe the central values. They represent the variability of the fitted results, defined in the following way.

The scope of these samarium measurements, using multiple sample thicknesses, experiment types (transmission or capture), and two energy regimes, is such that the final resonance parameters are derived from an overdetermined system. That is, any number of subsets of the overall data taken would be sufficient to specify the resonance parameters. Several subsets should reproduce the resonance parameters within the experimental uncertainty of each subset. Therefore, the variability of the resonance parameters resulting from SAMMY fits to different subsets of the overall data is a method to estimate the uncertainty on the resultant parameters. This method was used to determine the uncertainties given in parentheses in Table V for the present measurements for all resonances except those at 16, 23, 24.7 and 28 eV.

The uncertainties of resonance parameters for weak resonances, specifically resonances at 16, 23, 24.7, and 28 eV, were determined from SAMMY sensitivity studies. These resonances are predominantly capture and the goodness of fit as measured by χ^2 was found to be insensitive to Γ_γ over a wide range of values. For these resonances a series of SAMMY calculations was made to envelop the range of resonance parameters which fit the data with χ^2 within approximately 5% of each other. The uncertainties quoted in parentheses in Table V for the present measurements for these resonances are based on this criterion. This insensitivity was quantified by large uncertainties (up to 50%) in Γ_γ (see Table V). For these resonances where $\Gamma_\gamma >> \Gamma_n$, and for thin samples, RI is independent of Γ_γ. The neutron width, Γ_n, has a smaller uncertainty (less than 12%).

Resonance energies for resonances at 0.1, 0.9, and 3.4 eV were determined from a combined fit of all thermal transmission and thermal capture measurements. Resonance energies for the 5 and 6.4 eV resonances were determined from selected samples of both thermal and epithermal, transmission and capture data. The energies of the 8 and 9 eV resonances were determined from 0.025-mm thick thermal transmission data. Resonance energies for resonances from 12 to 30 eV were fitted using all epithermal transmission and capture samples. Spin assignments for the resonances analyzed were not varied.

The uncertainties on the resonance energies are based on judgement of the accuracy of flight path lengths and corresponding discrepancies between different experiments (capture and transmission, epithermal and thermal) which measure slightly different energies for the same resonances. These uncertainties in resonance energies are estimated to be 0.01 eV for all resonances except the 0.096 ± 0.001 eV resonance.

Systematic errors are those which are common to both capture and transmission measurements. The transmission and capture measurements are independent and complimentary methods for determining resonance parameters. Common features to both types of experiments and possible sources of systematic uncertainties include using the same electron accelerator, the same neutron-producing target, the same method for determining flight path length, some of the same Sm samples, and some of the same data acquisition electronics. Other potential sources of error include capture flux normalization or the analytical descriptions of the resolution functions.

The measurement of the 0.1 eV resonance has not changed the resonance integral or the thermal capture cross-section significantly. This is a result of the offsetting effects of smaller Γ_n and slightly lower resonance energy. The neutron width of the 0.1 eV resonance is 4% lower than ENDF (0.507 meV vs. 0.529 meV). However, the contribution to an individual resonance to the resonance integral and to the thermal capture cross-section are proportional to E^{-2} and $E^{-5/2}$, respectively. Therefore, the slight shift in resonance energy (from 0.0981 eV to 0.096 eV) compensates for the smaller Γ_n.

The resonance parameters presented here fit data from multiple sample thicknesses and six independent experiments rather well. The statistical uncertainties in resonance parameters are generally smaller than those of prior measurements (see Table V). The apparent increases in resonance integrals given in Tables VI and VII are within the uncertainties of the measurements. The measured resonances account for 99% of the extended resonance integral. Similarly, the apparent increase in the thermal capture cross-section is within the uncertainty of the measurements. The measured resonances contribute 65% of the thermal capture cross-section.

VI. CONCLUSIONS

The measurement and analysis of samarium capture and transmission data at the RPI LINAC has improved the accuracy and understanding of the neutron cross-section parameters. Five samples were measured in capture at the 25 meter flight station using a multiplicity-type capture detector. Data were analyzed up to 30 eV. Three transmission experiments, which measure total cross-section, were also performed on eleven different Sm samples at either the 15-m or the 25-m flight station and analyzed up to 30 eV.

Resonance parameters were extracted from combined capture and transmission data sets using the multi-level R-matrix Bayesian code SAMMY. The analysis included Doppler broadening, resolution broadening and multiple scattering correction of capture data. Separate resolution functions for transmission and capture were used.

The present measurements assumed the same spin assignments as ENDF for all resonances analyzed. The resonance integral, expanded to include the 0.1 eV resonance, is statistically unchanged from the ENDF evaluation. The effect on total thermal cross-section is also within experimental uncertainties of that obtained from ENDF parameters.

The results of the SAMMY calculations fit our experimental data better than the ENDF parameters (see Figures 1-5). State-of-the-art detectors, electronics, and analysis tools have allowed us to reliably update the database of elemental samarium resonance parameters. The more accurate knowledge of individual resonance parameters will allow nuclear designers to more accurately evaluate the neutronics effects of samarium in a reactor.

REFERENCES

1 R. E. SLOVACEK, R. C. BLOCK, Y. DANON, C. WERNER, G.-U. YOUK, J. A. BURKE, N. J. DRINDAK, F. FEINER, J. A. HELM, K. W. SEEMANN, "Neutron Cross-Section Measurements at the Rensselaer LINAC," *Proc. Topl. Mtg. Advances in Reactor Physics*, April 11-15, 1994, Knoxville, Tennessee, Vol. II, p. 193, ANS (1994).

2 R. C. BLOCK, P. J. MARANO, N. J. DRINDAK, F. FEINER, K. J. SEEMANN, and R. E. SLOVACEK, "A Multiplicity Detector for Accurate Low-Energy Neutron Capture Measurements," *Proc. Int. Conf. Nuclear Data for Science and Technology*, May 30-June 3 1988, Mito, Japan, p. 383.

3 M. E. OVERBERG, B. E. MORETTI, R. E. SLOVACEK, R. C. BLOCK, "Photoneutron Target Development for the RPI Linear Accelerator," *Nucl. Instrum. & Meth. Physics Research A*, **438**, 253 (1999).

4 Y. DANON, R. E. SLOVACEK, and R. C. BLOCK, "The Enhanced Thermal Neutron Target at the RPI LINAC," *Trans. Am. Nucl. Soc.*, **68**, 473 (1993).

5 Y. DANON, R. E. SLOVACEK, and R. C. BLOCK, "Design and Construction of a Thermal Neutron Target for the RPI LINAC," *Nucl. Instrum. & Methods Physics Research A*, **352**, 596 (1995).

6 N. M. LARSON, "Updated Users' Guide for SAMMY: Multilevel R-Matrix Fits to Neutron Data Using Bayes' Equations," ORNL/TM-9179/R4, Lockheed Martin Energy Research Corp., Oak Ridge National Laboratory, (1998).

7 Y. DANON, C. J. WERNER, G. YOUK, R. C. BLOCK, R. E. SLOVACEK, N. C. FRANCIS, J. A. BURKE, N. J. DRINDAK, F. FEINER, and J. A. HELM, "Neutron Total Cross-Section Measurements and Resonance Parameter Analysis of Holmium, Thulium, and Erbium," *Nucl. Sci. Eng.*, **128**, 61 (1998).

8 R. C. BLOCK, R. E. SLOVACEK, C. J. WERNER, J. A. BURKE, N. J. DRINDAK, and G. LEINWEBER, "Neutron Total and Capture Cross-Section Measurements and Resonance Parameter Analysis of Tungsten from 0.01 to 200eV," *Proc. Int. Conf. on the Physics of Nuclear Science and Technology*, October 5-8, 1998, Brookhaven, Long Island, New York.

9 G. LEINWEBER, J. BURKE, C. R. LUBITZ, H. D. KNOX, N. J. DRINDAK, R. C. BLOCK, R. E. SLOVACEK, C. J. WERNER, N. C. FRANCIS, Y. DANON, and B. E. MORETTI, "Neutron Capture and Total Cross-Section Measurements and Resonance Parameter Analysis of Zirconium up to 2.5 keV," *Nucl. Sci. Eng.*, **134**, 50 (2000).

10 R. C. BLOCK, Y. DANON, C. J. WERNER, G. YOUK, J. A. BURKE, N. J. DRINDAK, F. FEINER, J. A. HELM, J. C. SAYRES, and K. W. SEEMANN, "Neutron Time-of-Flight

Measurements at the Rensselaer LINAC," *Proc. Int. Conf. Nuclear Data for Science and Technology*, May 9-13, 1994, Gatlinburg, Tennessee, Vol. 1, p. 81, American Nuclear Society (1994).

11 D.K. OLSEN, G. DE SAUSSURE, R.B. PEREZ, F.C. DIFILIPPO, R.W. INGLE, and H. WEAVER, "Measurement and Resonance Analysis of Neutron Transmission Through Uranium-238," *Nucl. Sci. Eng.*, **69**, 202 (1979).

12 M. E. OVERBERG, "Development of an Improved Epi-thermal Neutron Target and Measurement of the Resolution Function to 350 eV," MS Thesis, Rensselaer Polytechnic Institute (1997).

13 Y. DANON, "Design and Construction of the RPI Enhanced Thermal Neutron Target and Thermal Cross-Section Measurements of Rare Earth Isotopes," PhD Thesis, Rensselaer Polytechnic Institute (1993).

14 D. B. SYME, "The Black and White-Filter Method for Background Determination in Neutron Time-of-Flight Spectrometry," *Nucl. Instrum. and Methods*, **198**, 357 (1982).

15 P. F. ROSE and C. L. DUNFORD, "ENDF-102 Data Formats and Procedures for the Evaluated Nuclear Data File ENDF-6," BNL-NCS-44945, Rev. 2, Brookhaven National Laboratory (1997).

16 S. F. MUGHABGHAB, *Neutron Cross Sections,* Vol. 1, Part B, Academic Press, Orlando, Florida (1984).

17 V. McLANE, P. F. ROSE, and C. L. DUNFORD, *Neutron Cross Sections*, Vol. 2, Academic Press, New York (1988).

18 H. M. MARSHAK and V. L. SAILOR, *Phys. Rev.*, **109**, 109 (1958).

19 N. J. PATTENDEN, *Proc. 2nd Int. Conf. Peaceful Uses Atomic Energy*, 1958, Vienna, Vol. 16, p. 44, IAEA (1958).

20 E. SOKOLOWSKI, H. PEKAREK, E. JONSSON, "Cross Section Measurements for Some Elements Suited as Thermal Spectrum Indicators, Cd, Sm, Gd, and Lu," *Nukleonik*, **6**, 245 (1964).

21 OE. R. AKYUEZ, C. CANSOY, F. DOMANIC, Y. OERGEEVREN, "Parameters for the First and Second Neutron Resonances in Sm-149," *Report CNAEM-52* (1968).

22 T. ASAMI, K. OKAMOTO, K. IDENO, and Y. OHNO, "The Parameters of the 0.099-eV Neutron Resonance in Sm-149," *Jour. Phys. Soc. Japan*, **26**, no. 2, 225 (1969).

23 N. J. PATTENDEN, "Neutron Cross Section Measurements on Fission Product Samarium and Iodine," *Nucl. Sci. Eng.*, **17**, 371 (1963).

24 J. W. CODDING, JR., R. L. TROMP, and F. B. SIMPSON, "Total Neutron Cross Section and Resonance Parameters of Promethium-147," *Nucl. Sci. Eng.*, **43**, 58 (1971).

25 H. M. EILAND, S. WEINSTEIN, and K. W. SEEMANN, "Neutron Cross Sections of Samarium-147 and Samarium-150," *Nucl. Sci. Eng.*, **54**, 286 (1974).

26 M. MIZUMOTO, "Neutron Resonance Parameters and Radiative Capture Cross Sections of Sm-147 and Sm-149," *Jour. Nucl. Phys. A*, **357**, 90 (1981).

27 F. RAHN, H. S. CAMARDA, G. HACKEN, W. W. HAVENS JR, H. I. LIOU, J. RAINWATER, M. SLAGOWITZ, S. WYNCHANK, "Neutron Resonance Spectroscopy. IX. The Separated Isotopes of Samarium and Europium," *Phys. Review C (Nucl. Phys.)*, **6**, no. 1, 251 (1972).

28 V. A. ANUFRIEV, T. S. BELANOVA, YU. S. ZAMJATNIN, A. G. KOLESOV, S. N. NIKOLSKIJ, V. A. PORUCHIKOV, S. M. KALEBIN, V. S. ARTAMONOV, R. N. IVANOV, "Measurement of the Total Neutron Cross Sections and Resonance Parameters of Pm-147, Sm-149," *Jour. Atomnaja Energija*, **44** (1978).

29 A. B. POPOV, K. TSHETSYAK, KHVAN-CHER-GOU, "Improved Parameters of Some Resonances of Sm and Dy," *Jour. Soviet Nucl. Phys.*, **32**, 310 (1980).

30 G. GEORGIEV, YU. S. ZAMYATNIN, L. B. PIKELNER, G. V. MURADIAN, YU. V. GRIGORIEV, T. MADJARSKI, N. JANEVA, "Determination of ^{147}Sm and ^{148}Sm Resonance Parameters," *Jour. Nucl. Phys. A*, **565**, 643 (1993).

31 V. A. ANUFRIEV, A. G. KOLESOV, C. I. BABICH, V. A. PORUCHIKOV, JU. B. NOVIKOV, V. A. SAFONOV, "Neutron Resonances of Sm-150 and Sm-151 Isotopes," *Proc. 4th All Union Conf. Neut. Phys.*, April 18-22, 1977, Kiev, USSR, Vol. 2, p. 263.

32 G. P. GEORGIEV, YU. V. GRIGORIEV, YU. S. ZAMYATNIN, G. V. MURADYAN, L. B. PIKELNER, KH. FAYKOV-STANCHIK, N. B. YANEVA, "Sm-149 Neutron Resonance Parameters Determination by the Method of the Gamma-Quanta Multiplicity," *Joint Inst. for Nucl. Res., Dubna Report-* P3-92-346, USSR (1992).

33 J. R. PARRINGTON, H. D. KNOX, S. L. BRENEMAN, E. M. BAUM, and F. FEINER, "Chart of the Nuclides," 15th Edition, General Electric Co. and KAPL, Inc. (1996).

34 JENDL-3.2, Japanese Evaluated Neutron Data Library, November 1993.

35 R. E. MacFARLANE and D. W. MUIR, "The NJOY Nuclear Data Processing System Version 91," LA-12740-M, October 1994.

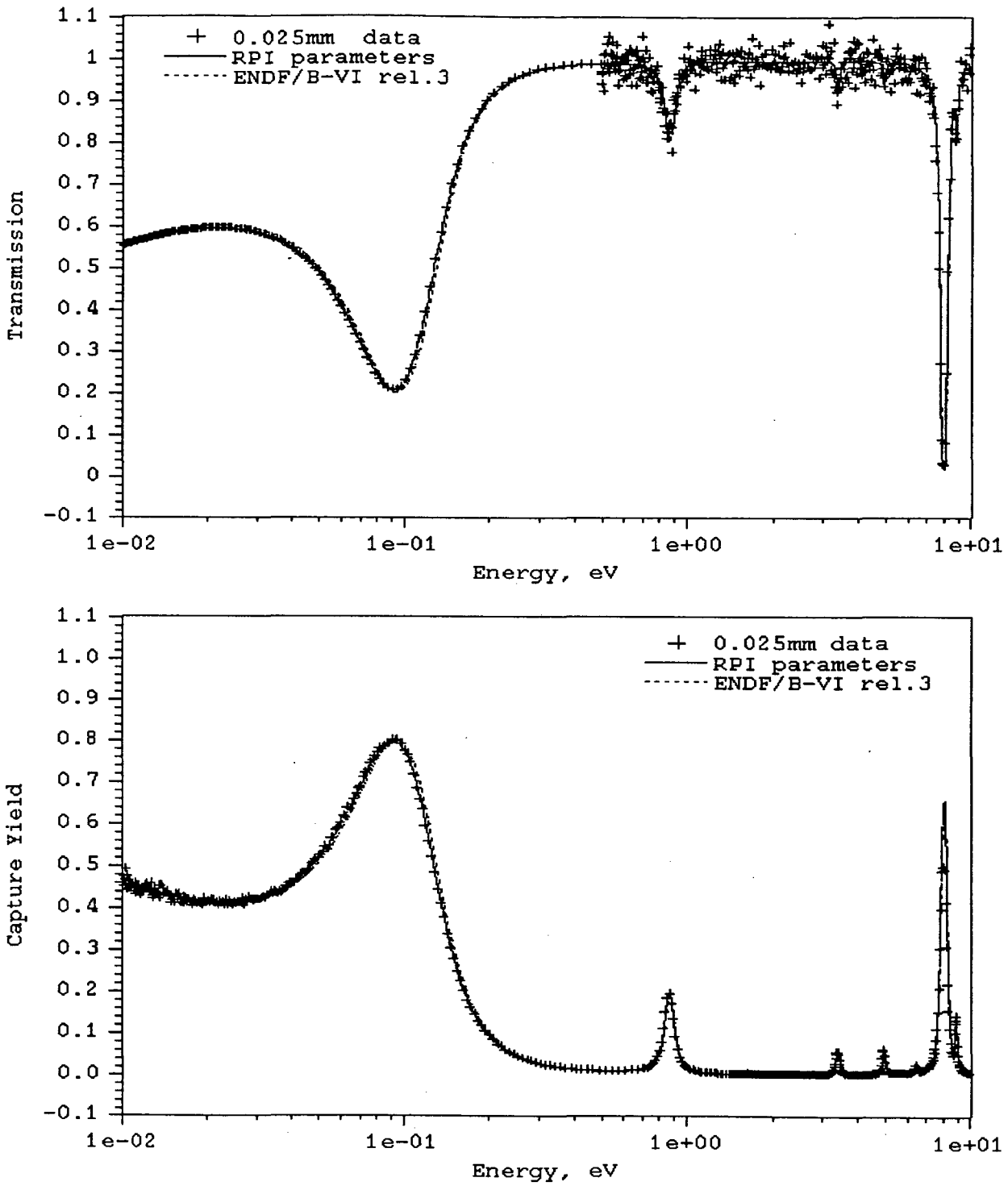

Fig. 1. Thermal Sm transmission and capture data. Compression of transmission data occurs at 0.5 eV. One in every five transmission data points below 0.5 eV is plotted. One in every ten transmission data points above 0.5 eV is plotted. Compression of capture data occurs at 1.4 eV. One in every five capture data points below 1.4 eV is plotted. One in every ten capture data points above 1.4 eV is plotted.

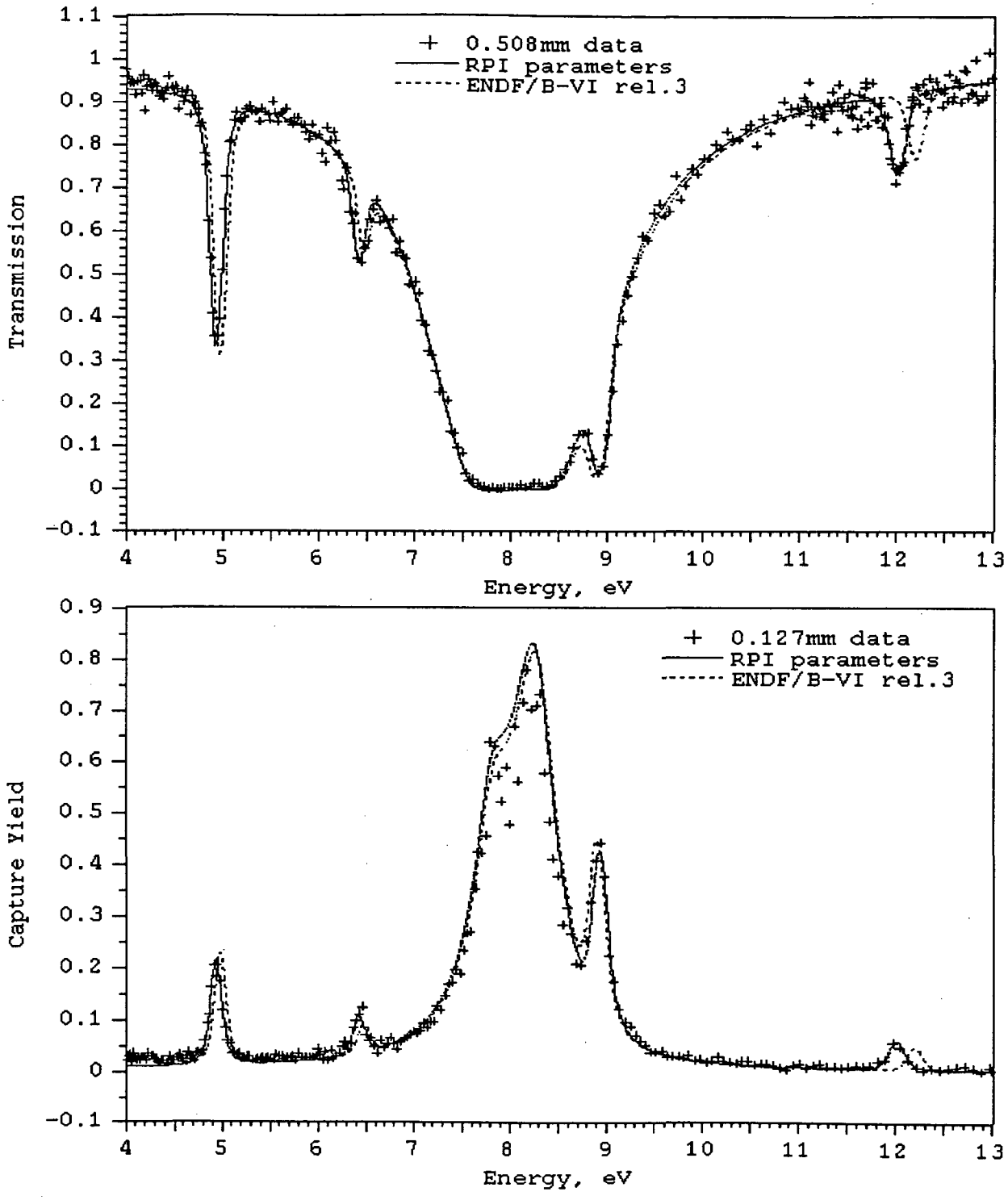

Fig. 2. Epithermal Sm transmission and capture data. All points below 6 eV are plotted. Compression occurs at 6 eV. Above 6 eV one in every eight capture data points is plotted. From 6 to 11 eV one in every eight transmission data points is plotted. Above 11 eV one in every three transmission data points is plotted.

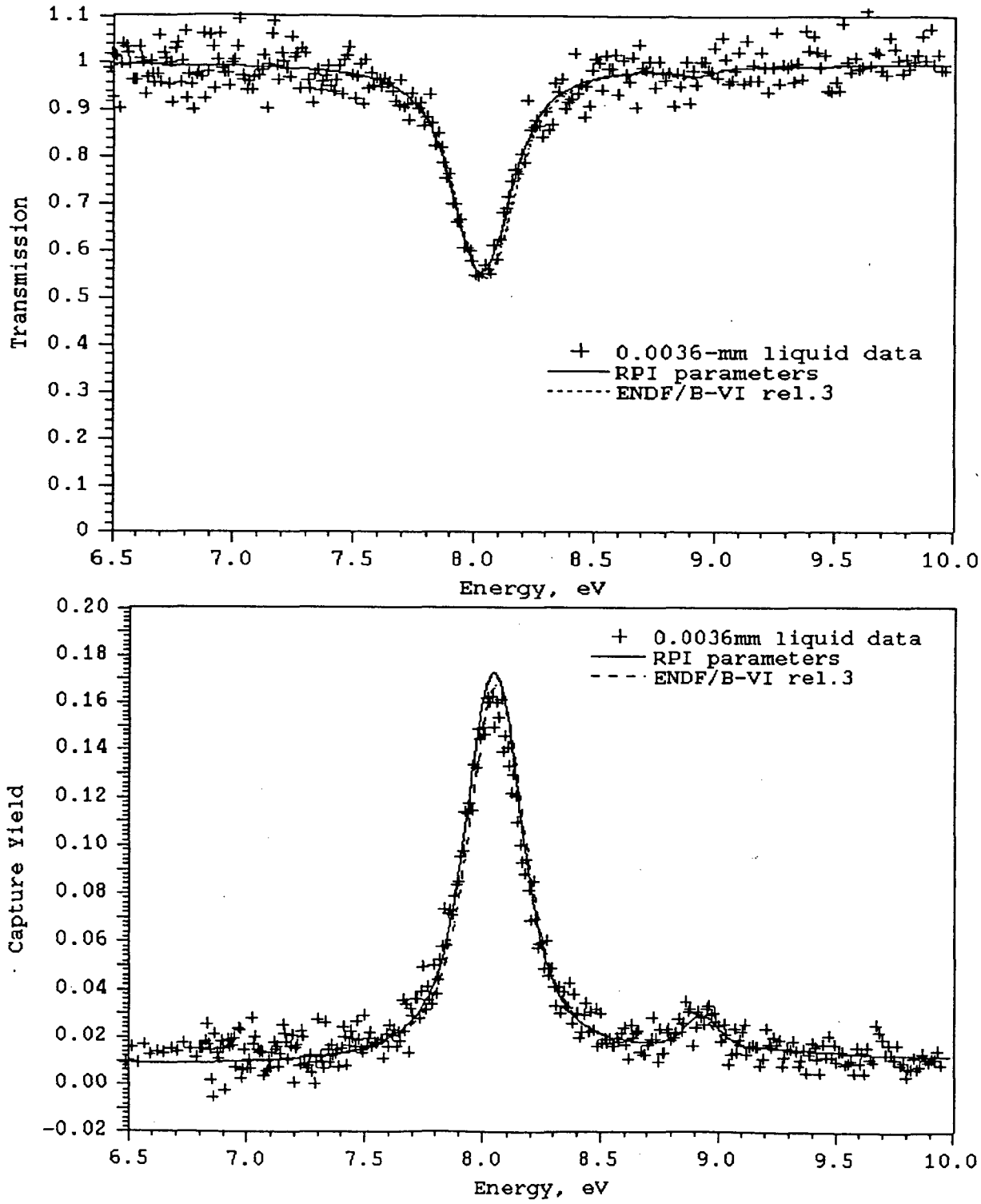

Fig. 3. 8.0-eV resonance in ^{152}Sm. Liquid sample data.
One third of transmission data and one half of capture data are plotted.

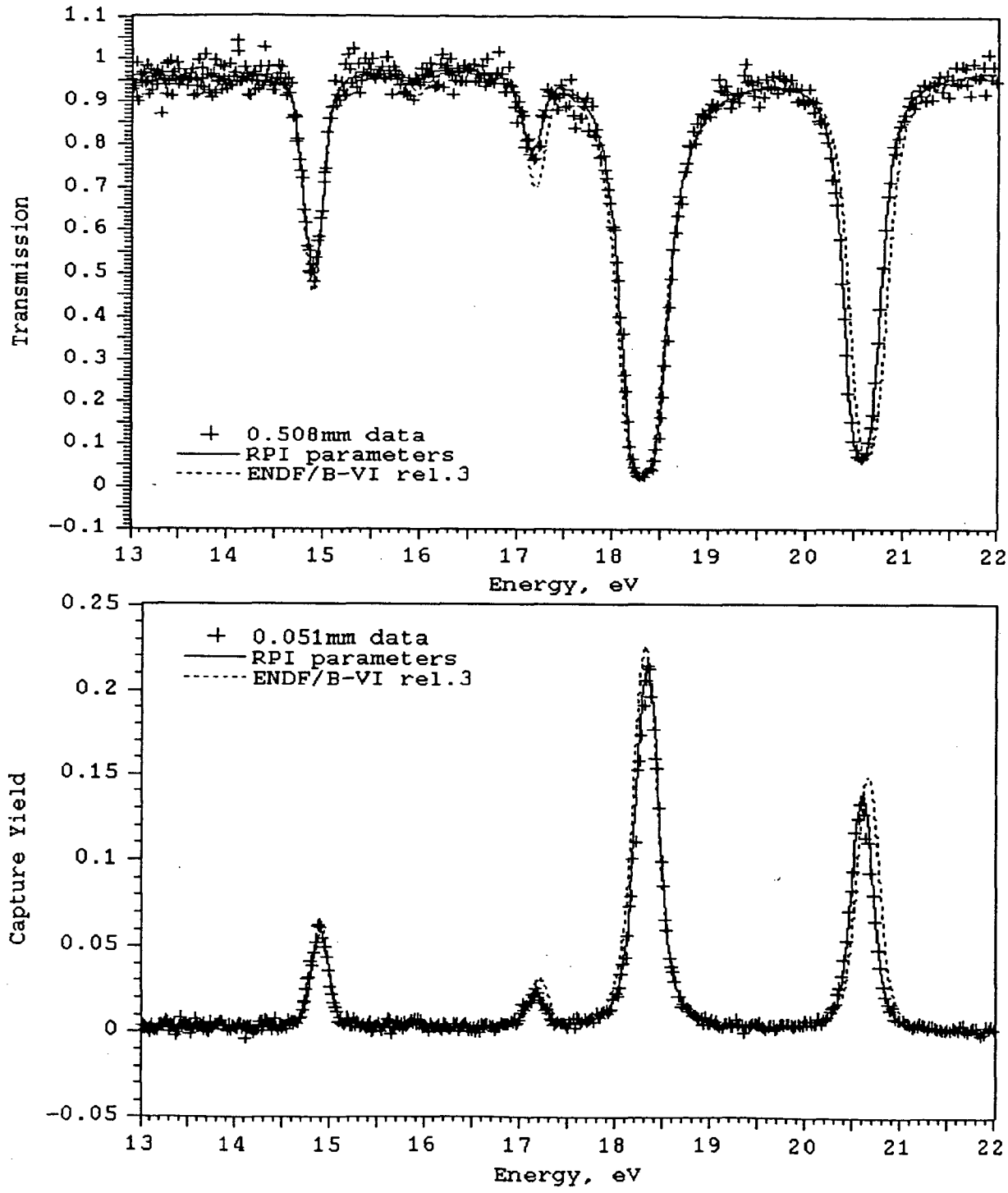

Fig. 4. Epithermal Sm transmission and capture data. All data points are plotted.

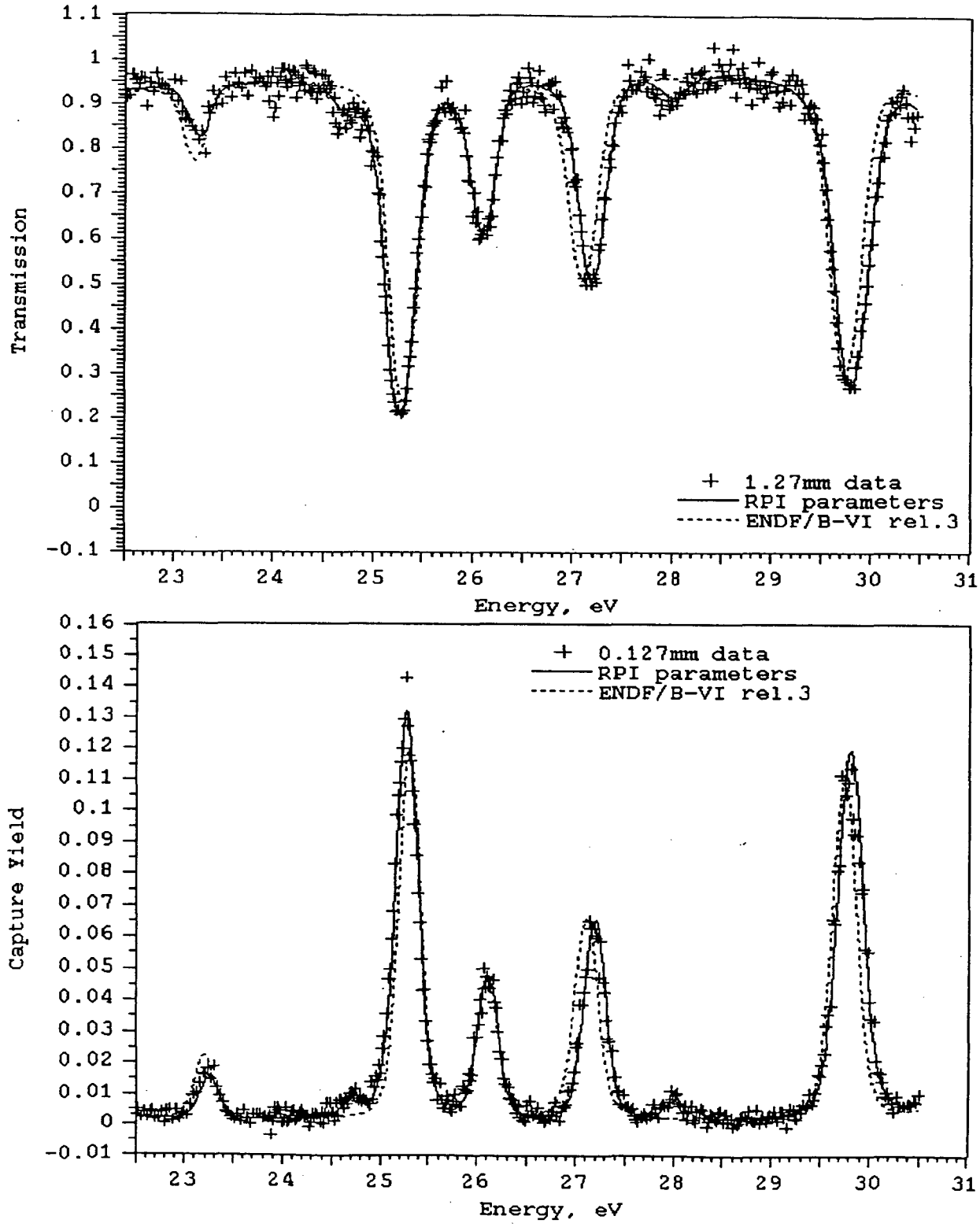

Fig. 5. Epithermal Sm transmission and capture data. All data points are plotted.